# Dual-mode camera using liquid-crystal microlens for high-resolution three-dimensional reconstruction

Lei Yu, Guo Fang

(School of Information Science & Technology, Shijiazhuang Tiedao University, Shijiazhuang 050043, China)

**Abstract:** A dual-mode camera (DMC) was proposed based on liquid-crystal microlens array (LCMLA), which could be readily switched between the conventional planar imaging mode and the plenoptic imaging mode through turning on/off the low frequency voltage signal applied on the LCMLA. The LCMLA was fabricated by common UV-photolithography and wet etching. Through coupling the LCMLA with a main lens and a photosensitive sensor array, a DMC prototype was constructed. Experiments were conducted to acquire plenoptic imaging data and corresponding planar imaging data of objects. The issues of the aperture design and the depth of field in the two modes were discussed in detail. A computation method for three-dimensional (3D) information acquisition based on the plenoptic imaging mode was given. A high-resolution 3D reconstruction was implemented by fusing 3D plenoptic data and corresponding 2D high-resolution planar imaging data.

**Key words:** plenoptic imaging; liquid-crystal microlens array; 3D reconstruction

**CLC number:** TN256 **Document code:** A **DOI:** 10.3788/IRLA20190540

# 使用液晶微透镜的高分辨率三维重建双模相机

雷 宇, 郭 芳

(石家庄铁道大学 信息科学与技术学院, 河北 石家庄 050043)

**摘 要:** 提出了一种基于液晶微透镜阵列的双模成像相机。该相机通过打开或者关闭加载在液晶微透镜阵列上的低频电压信号可以快捷地在传统平面成像模式和光场成像模式之间进行切换。液晶微透镜阵列通过常规紫外光刻和湿法刻蚀技术制作而成。通过将液晶微透镜阵列和感光传感器阵列以及主镜头耦合到一起,构造了一个双模成像相机的原型。通过该双模成像相机开展了相关实验,获取了同一目标物的光场图像和平面图像,并对孔径设计和两种工作模式下的景深进行了分析,给出了光场成像模式下目标物三维信息的计算方法,通过将三维光场数据和对应二维平面数据的信息进行融合获得了高分辨率三维图像。

**关键词:** 光场成像; 液晶微透镜阵列; 三维重建

**收稿日期:** 2020−05−24; **修订日期:** 2020−06−11

**基金项目:** 国家自然科学基金 (61972267)

**作者简介:** 雷宇 (1977−), 男, 讲师, 博士, 主要从事三维图像获取方面的研究工作。 Email: leiyu4983@126.com

## 0 Introduction

Currently, there are mainly three types of imaging devices to acquire the three dimensional (3D) information of the static and dynamic world around us, which are structured light cameras, time-of-flight cameras and multiple synchronous cameras [1−4]. However, these imaging devices all suffer from complicated configurations and high costs. The newly-developed portable plenoptic camera can also be used to record the 3D information of the objects [5−9]. Generally, a plenoptic camera can be constructed by inserting a microlens array (MLA) between the main lens system and the imaging sensor in a conventional camera. However, the rendered images restored from plenoptic cameras have a disappointingly low resolution because a large proportion of the sensor for direction resolving is already taken up. Boominathan et al. showed a hybrid imaging system consisting of a plenoptic camera and a traditional digital single lens reflex camera to achieve high-resolution digital refocusing, but the hybrid system is not portable [10].

Generally, typical plenoptic cameras mentioned above utilize traditional MLA. In recent years, liquid-crystal microlens arrays (LCMLAs) have sprang up as a potential substitution for MLA [11−13]. So far, nematic LC materials have been widely used in LC lens applications. Nematic LC molecules are rod-like and their long molecule axis can be preferably oriented in a special direction. The nematic LC materials sealed in two electrodes will reorient their directors along the electric-field direction stimulated in LC layer. If the stimulated electric-field is nonuniform radially, a gradient index lens can be shaped due to the variance of the tilting angles of LC molecules.

In this paper, a dual-mode plenoptic camera (DMC) used for 3D reconstruction of static scene based on the LCMLA is proposed. When a voltage signal with needed RMS value is applied between the electrodes of the LC device, the DMC will present a plenoptic imaging mode for acquiring 3D radiation parameters of objects. If the voltage signal is turned off, the DMC will be a traditional camera so as to exhibit a dual-mode imaging feature. Through fusing the 3D plenoptic data and corresponding high-resolution planar data of the same objects, a high-resolution 3D reconstruction can be achieved effectively so as to highlight a way to remarkably increase the 3D imaging resolution based on the LCMLA-sensor chip with a dual-mode imaging ability.

## 1 DMC

### 1.1 Microstructure of the LCMLA

The LCMLA is the key component of the DMC. In plenoptic mode, it acts as the microlens array which can focus the incident rays onto the sensor. Moreover, it must permit the transmittance of the rays in the planar mode. The appropriate materials are chosen and the structure is designed as shown in Fig.1(a). It includes two glass substrates with a thin indium tin oxide (ITO) layer on them as the electrodes. The thicknesses of the glass substrate and the ITO layer are ~500 μm and ~50 nm separately, and the square resistance of the ITO film is ~200 Ω. The ITO layer of the top substrate is etched with an array of circular holes with the diameter of 128 μm and the hole pitch of 160 μm via UV-photolithography and wet etching, whereas the bottom substrate is not etched. Both the top and the bottom substrates are coated with a polyimide (PI) layer by spin-coating. The PI layer of the electrodes are rubbed antiparallel to make the nematic LC

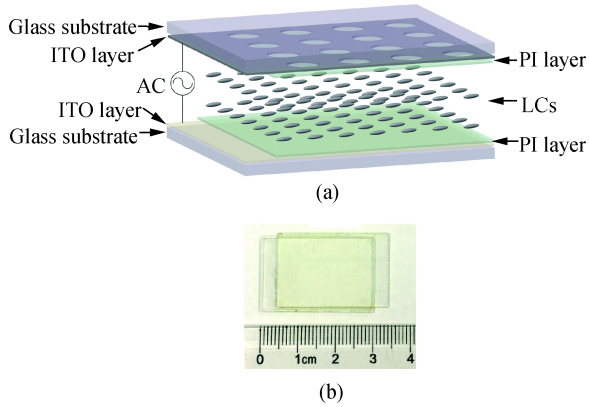


(a)

(b)

Fig.1 LCMLA device. (a) 3D structure (not in scale) and (b) an actual LCMLA with two conductive tapes

molecules instilled align in the same direction in the natural state. The electrodes are sealed face to face with an adhesive mixed with a number of 20-μm-diameter microspheres along the edges to form an inner 20-μm-thick microcavity for LC materials. Figure1(b) shows an actual LCMLA developed by ourselves.

Generally, LC materials present obvious birefrigent. The angle between the optic axis and beam propagation direction determines the refractive index $n_e$ with respect to extraordinary rays, but does not affect the refractive index $n_o$ of ordinary rays (usually $n_e > n_o$). When a voltage signal is applied between two electrodes of the LCMLA constructed, a radially nonuniform electric-field will be generated in each microlens, which means that the electric-field intensity will be increased gradually from the center to the edge, and then the reorientation of LC molecules will also present a similar variance trend. If an appropriate signal voltage is applied, the refractive index for extraordinary rays will decrease from $n_e$ at the center to $n_o$ nearing the edge in each microlens. Therefore, an array of gradient index microlenses is formed to converge incident extraordinary rays.

As shown in experiments, the variance of the electric-field stimulated in LC layer will result in a change of the focal length in a relatively small range. The LC material used by us is E44 from Merck, and their indexes are $n_o$=1.523 and $n_e$=1.778. An experimental relation between the focal length and the applied RMS voltage is shown in Fig.2. A square-wave signal with a frequency of 1 kHz is employed to drive the LCMLA. Their focal length can be shifted in a range of ~1.55 mm to ~2.15 mm when the voltage signal is in the range from ~3.0 $V_{rms}$ to ~15.0 $V_{rms}$. If the voltage signal is more than a value of ~15.0 $V_{rms}$, the electric-field intensity will be too strong to generate an effective spatial refractive index distribution. It should be noted that not all voltage signal between ~3.0 $V_{rms}$ and ~15.0 $V_{rms}$ can lead to an ideal imaging quality. According to our experiments, ~7.0 $V_{rms}$ is a typical RMS value for generating a fairly sharp object image. Since the aim of performing electrically tuning focal length is only to acquire an ideal imaging quality, the voltage signal of ~7.0 $V_{rms}$ is chosen as a common RMS value for driving our DMC in experiments. Thus the focal length of the LCMLA in our DMC is ~1.55 mm.

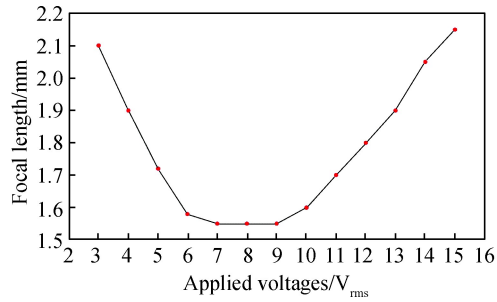


Fig.2 Focal length vs the signal voltage applied over the LCMLA fabricated by us

### 1.2 Layout of the DMC

The schematic layout of the DMC is shown in Fig.3. It principally includes three components, the main lens system, the LCMLA, and the imaging sensor. Incident rays coming from objects are converged firstly by the main lens system. In the planar imaging mode, beams passing through the LCMLA will maintain their propagation directions but still experience a very small phase delay in the optical axis direction. A real image will be formed at the imaging plane through the main lens system. The sensor should be positioned at the imaging plane for capturing sharp images. Considering an ideal lens system, a relationship between the object distance $a_L$ and the image distance $b_L$ satisfies a common thin lens equation as the following.

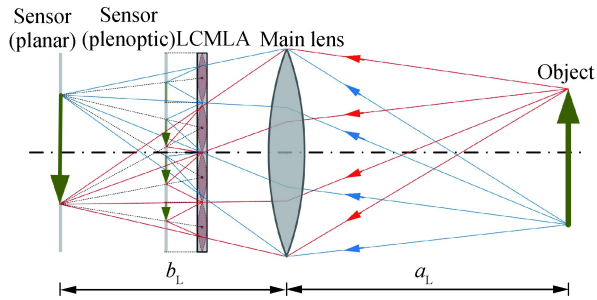


Fig.3 Layout of the DMC (not in scale)

$$\frac{1}{f_L} = \frac{1}{a_L} + \frac{1}{b_L} \tag{1}$$

where $f_L$ represents the focal length of the main lens system.

In the plenoptic imaging mode, incident rays passing through the LCMLA will be bent and then focused onto the plenoptic imaging plane before reaching the real imaging plane of the main lens system. In this occasion, the sensor should be moved towards the main lens system to acquire raw imaging data of the object. It is obvious that the rays from the same object point are split by several adjacent LC microlenses and then generate several image points on the sensor. A pinhole model is used to determine the exact positions of these points. Thus, each microlens can image the whole or part of the real object. The micro image generated by each microlens is called an elemental image. It is evident that the elemental images are overlapped and then the overlapping extent is determined by the triangulation of the DMC and the distance of the object point from the DMC. It is obvious that one object point is projected as one image point in the planar imaging mode, whereas multiple image points in the plenoptic imaging mode. Thus, the resolution of the rendered image restored from raw imaging data obtained in the plenoptic imaging mode is reduced sharply than that captured in the planar imaging mode.

It should be noted that the LCMLA and the sensor in our model is all set before the real image plane of the main lens system, and then the LCMLA will project a virtual object into a real image. However, they can also be put at an appropriate position behind the real image plane of the main lens system, which means that a real image can be formed before the relay imaging. Its theoretical model is almost the same as our model, and only our model is discussed carefully in the following.

Figure 4 shows the DMC prototype constructed for 3D high-resolution reconstruction. The size of the sensor is 4 384×3 288 with a pixel pitch of 1.4 μm, which is connected with a computer to save the raw image data acquired. The LCMLA is powered by a LC Controller developed by ourselves, which provides a stable square-wave voltage signal with an RMS value ranging from 0 to 30.0 $V_{rms}$ and a frequency of 1 kHz. An oscilloscope is adopted to monitor the applied voltage signal. The LCMLA is coupled tightly onto the surface of the protecting window of the sensor, and the distance between the LCMLA and the photosensitive surface of the sensor is ~1.3 mm. The LCMLA-sensor are fixed onto a three-dimensional stage. The main lens system with a focal length of 35 mm is just located before the LCMLA-sensor so as to construct a DMC prototype. To filter the ordinary rays of incident beams, which will bring relatively strong noise into plenoptic imaging signals, a polarizer is inserted in the measured light-path.

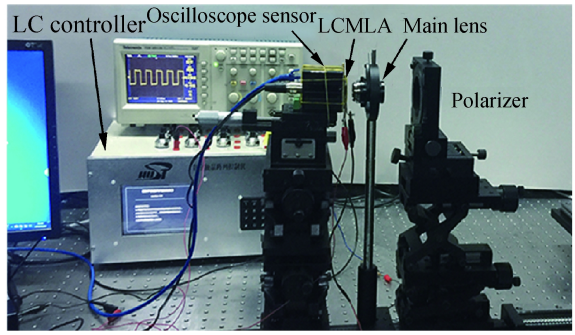


Fig.4 DMC prototype

### 1.3 Aperture of the main lens system

In the plenoptic imaging mode, the aperture of the main lens system is a determinant factor for the size selection of elemental images. Figure 5 shows several typical cases when the size of elemental images is changed with the aperture of the main lens system. As shown in Fig.5(a), the sensor coupled with the microlenses are not fully utilized because the aperture is too small. To utilize the sensor to the maximum, adjacent elemental images should be tangent without any overlapping, as shown in Fig.5(b). If the aperture of the

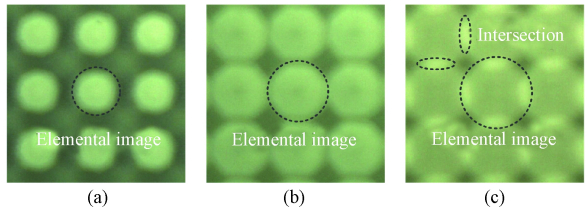


(a) (b) (c)

Fig.5 Elemental images acquired when the aperture is, (a) small, (b) suitable, and (c) large

main lens system is too large, adjacent elemental images will overlap as shown by Fig.5(c).

As shown in Fig.6, the rays propagating towards the virtual image point I are converged by several microlenses of the LCMLA in the image space of the main lens. If the cone of the rays covers the microlens *A* and *F*, the real image points $I_a$ and $I_f$ will be generated which will invade the image fields of their adjacent microlens *B* and *E*. Therefore, the angle of the cone should not be larger than $\beta$, in order that the rays is confined in the area of microlens *B*, *C*, *D* and *E*, which will form real image points in their own image fields. If the coverage of the cone is smaller to the domain of *C* and *D*, the image points $I_b$ and $I_e$ will not be formed and the corresponding positions on the sensor will be dark resulting in a waste of the sensor.

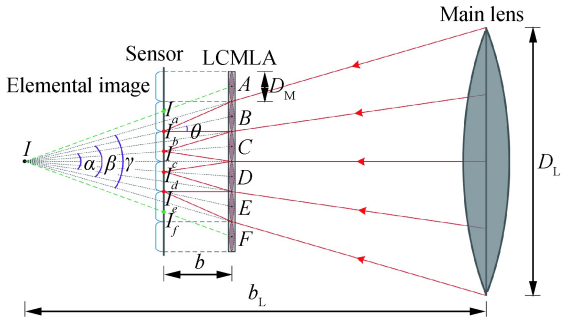


Fig.6 Typical imaging process of the DMC prototype constructed

Since the aperture of each microlens is very small, the angle $\beta$ satisfying the relation $\alpha<\beta<\gamma$ can be taken approximately. According to the triangulation, $\beta = 2\theta$, a relation between the main lens system and microlenses can be obtained as

$$\frac{D_{\mathrm{L}}}{b_{\mathrm{L}}} \approx \frac{e}{b} \tag{2}$$

where $D_{\mathrm{L}}$ and *e* represent the aperture of the main lens system and LC microlens respectively, and *b* represents the distance between the sensor and the LCMLA. Therefore, the *F*/numbers of the main lens system and each microlens should be matched carefully in the plenoptic imaging mode and the chief ray angle (CRA) is calculated to be 4.3°. Although there is no aperture limitation to the main lens system in the planar imaging mode, the aperture is recommended to be the same with that in the plenoptic imaging mode for fast switching between the two imaging modes.

### 1.4 DOF comparison of two modes

According to the imaging architecture constructed, we can expect that two factors affecting imaging resolution of the DMC are the pixel pitch and the radius of Airy disk. A symbol *s* is used to represent the resolution limit of the DMC, which should be the larger one between the two factors mentioned above. Figure 7 shows part of the image space of the main lens system behind the LCMLA, where points $I_1$ to $I_5$ are five virtual image points formed by the main lens. The cone angles of incident rays towards the five points are approximately equal.

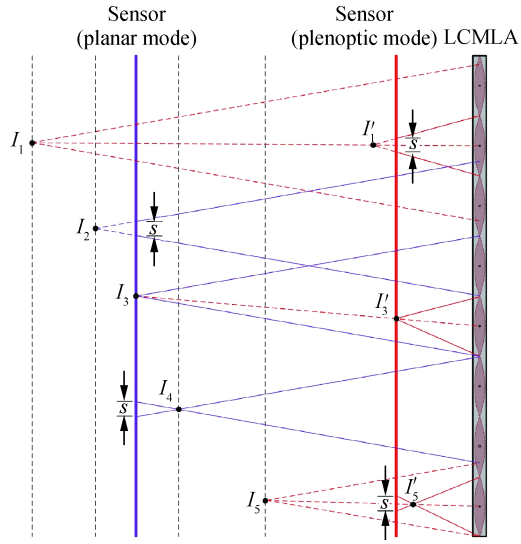


Fig.7 Partial image space of the main lens system that is behind the LCMLA (not in scale)

In the plenoptic imaging mode, only three image points $I_1$, $I_3$, and $I_5$ in the planar mode are considered which are effectively reimaged by corresponding microlenses, as shown by image points $I_1$', $I_3$', and $I_5$'. As shown, point $I_3$' is just on one sensor, while points $I_1$' and $I_5$' are behind and before the sensor and thus two blur spots are formed. If the blur spots are equal to or smaller than *s*, the spots can still be viewed as focus. Supposing the diameters of points $I_1$' and $I_3$' are equal to *s*, the refocused range of the microlenses is between the image

plane $I_1$ and $I_5$.

While in the planar imaging mode, the rays forming point $I_3$ is focused by the main lens system just onto the sensor, while points $I_2$ and $I_4$ are blur spots with size $s$. Therefore, the field between the plane $I_2$ and $I_4$ are acceptably sharp in this mode.

It is obvious that the DOF in the plenoptic imaging mode is much wider than that in the planar imaging mode, because the LCMLA not only divides the cone of incident rays but also recompresses the image space of the main lens.

### 1.5 Imaging efficiency of two modes

Three toy bricks are laid out as objects and imaging experiments in the two imaging modes mentioned above are conducted using the DMC developed. In the plenoptic imaging mode, the screw micrometers of the stage supporting the sensor and the LCMLA, as shown in Fig.4, are set to the same scale at every snapshot to assure the constancy of the DMC once its configuration parameters are determined, because the computation of 3D information of the objects relies on the geometry of the DMC, which will be discussed later.

Firstly, the LCMLA is supplied by a voltage signal of ~7.0 $V_{rms}$ and then the DMC acts as a plenoptic camera, as shown by Fig.8. Figure 8(a) presents a whole image including three objects with different objective distance. The close-ups of three bricks are shown by Fig. 8(b) to Fig.8(d). It can be seen that each microlens only images part of the objective space clearly, due to the wide DOF in the plenoptic mode. When the LCMLA is turned off, the DMC is switched to the planar imaging mode. The objects and the main lens system remain unchanged. Cautiously adapting the back-and-forth micrometer to make it to move along the optical axis direction, the assembly of the sensor and the LCMLA is moved backwards slowly so as to sequentially get the focuses of the bricks.

Figure 9 shows the planar images of the bricks in the planar imaging mode, which exemplify the narrower DOF of the planar mode than the plenoptic mode.

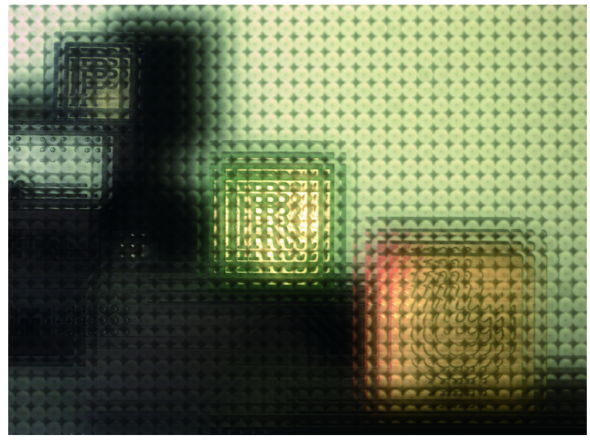

(a)

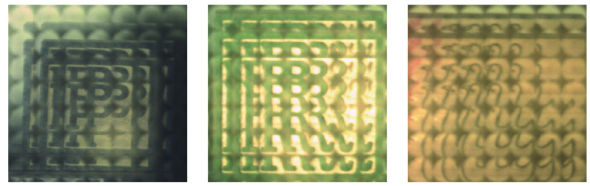

(b) (c) (d)

Fig.8 Plenoptic images. (a) Panorama image, (b) a close-up of the far brick, (c) a close-up of the middle brick, and (d) a close-up of the near brick

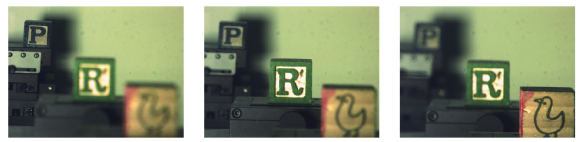

(a) (b) (c)

Fig.9 Typical imaging character of the planar imaging mode including: (a) far brick, (b) middle brick, and (c) near brick

## 2 3D reconstruction

### 2.1 Depth estimation in the plenoptic imaging mode

Before performing 3D reconstruction, sufficient 3D information must be figured out according to the DMC constructed. The objective distance or depth is a pivotal parameter for achieving fast calculation. To estimate the depth of a virtual object point formed by the main lens system in the plenoptic imaging mode, at least two real image points must be shaped on the sensor. According to the position of the image points originated from the same object point, a geometric relationship between the depth of the object point and its corresponding image point can be set up. Figure 10 presents a typical parameter arrangement for the depth estimation of 3D reconstruction.

As shown, the light rays propagating towards the virtual image point I formed by the main lens system are split by two adjacent microlenses and then converged onto the sensor so as to result in two real image points $I_1'$ and $I_2'$. The pinhole model is used to determine the position of the real image point. Points $O_1$ and $O_2$ are the projections of the principal points of the two microlenses onto the sensor. Two variables $d_1$ and $d_2$ are defined as the coordinates of the two real image points $I_1'$ and $I_2'$. Taking $O_1$ and $O_2$ as the origin points separately, a disparity variable $\Delta d$, which is the difference between $d_1$ and $d_2$, can be yielded as

$$\Delta d = |d_1 - d_2| \tag{3}$$

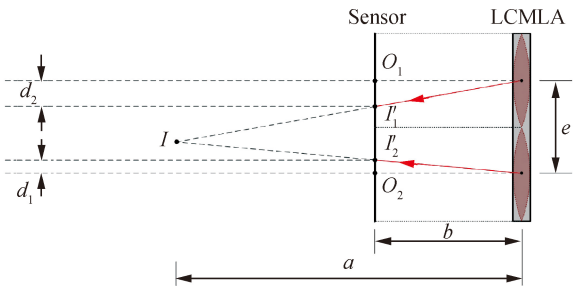


Fig.10 Parameter arrangement for the depth estimation of 3D reconstruction

According to the similar triangle theorem, an equation can be acquired as

$$b/a = \Delta d/e \tag{4}$$

where $a$ denotes the object distance with respect to the LCMLA, and can be calculated as

$$a = be/\Delta d \tag{5}$$

Since the practical values of $b$ and $e$ can be obtained from the configuration of the DMC, the disparity variable $\Delta d$ is a key factor, which can be measured according to image matching between the elemental images of adjacent microlenses. So far, several image matching algorithms have been developed including the sum of absolute differences (SAD), the sum of squared differences (SSD), and normalized correlation coefficient (NCC). Considering the complexity of matching a small pixel point, a window with an adaptable size is adopted. Figure 11 shows an example based on window matching between two adjacent microlenses according to the NCC method. So, the disparity $\Delta d$ between the two windows can be measured as 32.2 μm (23 pixels).

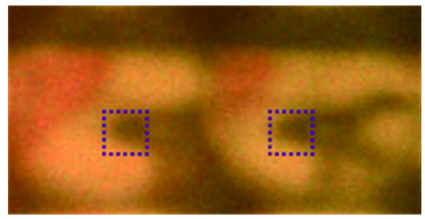

Fig.11 Window matching between two adjacent microlenses

### 2.2 3D positioning of real object point

After determining the depth of a virtual image point formed by the main lens system, the 3D coordinates of corresponding object points can be calculated according to the similar triangle theorem. As shown in Fig.12, the pinhole model is adopted to illustrate the position of an object point $P$, the virtual image point $I$, and one real image point $I'$. The $z$-axis of the coordinate system is normal to the sensor, whereas $x$- and $y$-axis are parallel to the sensor. The coordinates ($I'_x$, $I'_y$) of point $I'$ and ($L_x$, $L_y$) of principal point $L$ of the microlens can be obtained according to the DMC architecture. The coordinates ($I_x$, $I_y$) of point $I$ can be calculated by the equation of

$$\frac{L_x - I'_x}{L_x - I_x} = \frac{L_y - I'_y}{L_y - I_y} = \frac{a}{b} \tag{6}$$

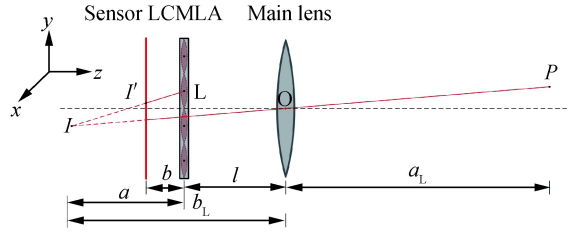


Fig.12 Parameter configuration for 3D positioning

According to the thin lens equation, the objective distance can be figured out by the relation of

$$a_L = 1/(1/f_L - 1/(a+l)) \tag{7}$$

where $l$ denotes the distance between the LCMLA and the main lens system. The coordinates ($P_x$, $P_y$) of object point $P$ can also be acquired finally from the equation of

$$\frac{P_x}{-I_x}=\frac{P_y}{-I_y}=\frac{a_{\mathrm{L}}}{b_{\mathrm{L}}} \tag{8}$$

To compute the 3D coordinates of a window setting in the plenoptic imaging mode, the parameters of $b$, $l$, and $f_{\mathrm{L}}$ should be measured manually. Moreover, to decrease the errors of the results, a thorough calibration must be done to figure out accurate values before the DMC is put into use.

### 2.3 Image matching between two imaging modes

After the coordinates of all windows have been calculated, the 3D reconstruction can be performed accordingly. However, the resolution in the plenoptic imaging mode is much lower than that in the planar imaging mode because a portion of the sensor has already been taken up by directional information. To achieve high-resolution 3D reconstruction, each window should be matched with the planar image to find out its sharper clip originated from the same space. In order to improve the correctness of image matching, several adjacent windows coming from the same depth can be synthesized together to form a larger patch.

In our experiments, three bricks with different depths are arranged along the optical axis. We can generate the patches of bricks from their windows and then match them with the planar images processed. Figure 13 shows a typical image matching operation between two modes. As shown in Fig.13(a), the patch of the near brick is rendered from the plenoptic image. Its matching clip of the planar image is shown in Fig.13(b). The lateral resolution between them is 1:5.25.

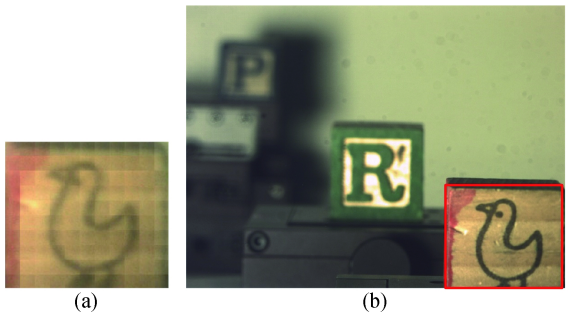

(a) (b)

Fig.13 Image matching between two imaging modes. (a) Patch of the near brick and (b) matching clip of the planar image

### 2.4 3D reconstruction

A high-resolution 3D reconstruction scene of the three bricks using corresponding clips of the planar images is shown in Fig.14. Compared with the plenoptic patches, the lateral resolution of the near, middle, and far brick is improved 5.25, 4.55, and 3.57 times, respectively.

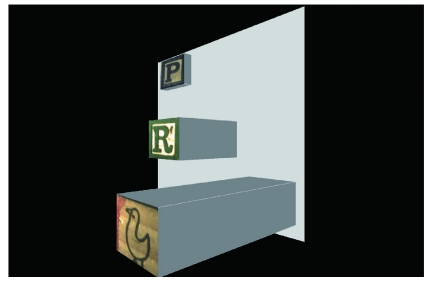

Fig.14 High-resolution 3D pattern reconstruction of the three bricks

## 3 Conclusion

In this paper, an imaging setup with a dual-mode function including the plenoptic imaging mode and the conventional planar imaging mode, is proposed. Two imaging modes can be switched easily by only turning on or off the voltage signal loaded over the LCMLA of the imaging setup. A camera architecture based on the constructed setup can further perform 3D high-resolution reconstruction through synthesizing 3D data acquired according to the plenoptic imaging mode and planar imaging data. Compared with 3D reconstruction only based on plenoptic imaging, our 3D reconstructive results improve the resolution greatly.

**References:**

[1] Zollhöfer Michael, Stotko Patrick, Görlitz Andreas, et al. State of the Art on 3D Reconstruction with RGB - D Cameras[C]// Eurographics, 2018, 37: 625-652.

[2] Lu Chunqing, Song Yuzhi, Wu Yanpeng, et al. 3D information acquisition and error analysis based on TOF computational image [J]. ***Infrared and Laser Engineering***, 2018, 47(10): 1041004. (in Chinese)

[3] Chen Ni, Zuo Chao, Byoungho Lee. 3D imaging based on depth measurement [J]. ***Infrared and Laser Engineering***, 2019, 48(6): 0603013. (in Chinese)

[4] Nonome Tomoaki, Sakaue Fumihiko, Sato Jun. Super-resolution 3d reconstruction from multiple cameras[C]//VISIGRAPP, 2018, 5: 481-486.

[5] Ng R, Levoy M, M. Brédif M, et al. Light field photography with a hand-held plenoptic camera [J]. ***Stanford Technical Report***, 2005, 2: 1-11.

[6] Lumsdaine A, Georgiev T. The focused plenoptic camera[C]//ICCP, 2009: 1-8.

[7] Perwass C, Wietzke L. Single lens 3D-camera with extended depth-of-field[C]//SPIE, 2012, 8291: 829108.

[8] Wang Jiahua, Du Shaojun, Zhang Xuanzhe, et al. Design of focused light field computational imaging system with four-types focal lengths [J]. ***Infrared and Laser Engineering***, 2019, 48(2): 0218003. (in Chinese)

[9] Chen Qi, Xu Xiping, Jiang Zhaoguo, et al. Light field computational reconstruction from focal planes based on light field camera [J]. ***Optics and Precision Engineering***, 2018, 26(3): 708-714. (in Chinese)

[10] Boominathan V, Mitra K, Veeraraghavan A. Improving resolution and depth-of-field of light field cameras using a hybrid imaging system[C]//ICCP, 2014, 1-10.

[11] Kang Shengwu, Tong Qing, Sang Hongshi, et al. Ommatidia structure based on double layers of liquid crystal microlens array [J]. ***Applied Optics***, 2013, 52(33): 7912-7918.

[12] Xin Zhaowei, Wei Dong, Xie Xingwang, et al. Dual-polarized light-field imaging micro-system via a liquid-crystal microlens array for direct three-dimensional observation [J]. ***Optics Express***, 2018, 26(4): 4035-4049.

[13] Lei Yu, Tong Qing, Zhang Xinyu. Light field imaging with a gradient index liquid crystal microlens array [J]. ***Infrared and Laser Engineering***, 2017, 46(2): 0220002.